Supercontinuum generation for coherent anti- Stokes Raman scattering microscopy with photonic crystal fibers

Pedersen, Pernille Klarskov; Isomäki, Antti; Hansen, Kim P.; Andersen, Peter E.

Published in:
Optics Express

Link to article, DOI:
10.1364/OE.19.026672

Publication date:
2011

Document Version
Publisher's PDF, also known as Version of record

Supercontinuum generation for coherent anti-Stokes Raman scattering microscopy with photonic crystal fibers

Pernille Klarskov,[1,*] Antti Isomäki,[1] Kim P. Hansen,[2] and Peter E. Andersen[1]

[1]*DTU Fotonik, Department of Photonics Engineering, Technical University of Denmark, Frederiksborgvej 399, 4000 Roskilde, Denmark*

[2]*NKT Photonics A/S, Blokken 84, DK-3460 Birkerød, Denmark*

[*]*pkpe@fotonik.dtu.dk*

Abstract: Photonic crystal fiber (PCF) designs with two zero-dispersion wavelengths (ZDWs) are experimentally investigated in order to suggest a novel PCF for coherent anti-Stokes Raman scattering (CARS) microscopy. From our investigation, we select the optimum PCF design and demonstrate a tailored spectrum with power concentrated around the relevant wavelengths for lipid imaging (648 nm and 1027 nm). This new PCF is characterized by varying the fiber length, the average power, and the pulse width of the fs pump pulses. It was found that the selected PCF design gave a significantly improved spectral distribution compared to an existing PCF for CARS microscopy. Furthermore, the PCF is designed in a twofold symmetric structure allowing for polarization maintaining propagation. Finally, the pulse propagation is investigated numerically showing good agreement with the measured spectrum. From the numerical analysis, the nonlinear effects responsible for the spectral broadening are explained to be soliton fission processes, dispersive waves, and stimulated Raman scattering.

OCIS codes: (060.4005) Microstructured fibers; (060.4370) Nonlinear optics, fibers; (190.5530) Pulse propagation and solitons; (300.6230) spectroscopy, coherent anti-Stokes Raman scattering; (320.6629) Supercontinuum generation.

References and links

1. R. F. Begley, A. B. Harvey, and R. L. Byer, "Coherent anti-Stokes Raman spectroscopy," Appl. Phys. Lett. **25**(7), 387–390 (1974).
2. J. Imitola, D. Côté, S. Rasmussen, X. S. Xie, Y. Liu, T. Chitnis, R. L. Sidman, C. P. Lin, and S. J. Khoury, "Multimodal coherent anti-Stokes Raman scattering microscopy reveals microglia-associated myelin and axonal dysfunction in multiple sclerosis-like lesions in mice," J. Biomed. Opt. **16**(2), 021109 (2011).
3. A. C. T. Ko, A. Ridsdale, M. S. D. Smith, L. B. Mostaco-Guidolin, M. D. Hewko, A. F. Pegoraro, E. K. Kohlenberg, B. Schattka, M. Shiomi, A. Stolow, and M. G. Sowa, "Multimodal nonlinear optical imaging of atherosclerotic plaque development in myocardial infarction-prone rabbits," J. Biomed. Opt. **15**(2), 020501 (2010).
4. R. K. Lyn, D. C. Kennedy, S. M. Sagan, D. R. Blais, Y. Rouleau, A. F. Pegoraro, X. S. Xie, A. Stolow, and J. P. Pezacki, "Direct imaging of the disruption of hepatitis C virus replication complexes by inhibitors of lipid metabolism," Virology **394**(1), 130–142 (2009).
5. X. Nan, A. M. Tonary, A. Stolow, X. S. Xie, and J. P. Pezacki, "Intracellular imaging of HCV RNA and cellular lipids by using simultaneous two-photon fluorescence and coherent anti-Stokes Raman scattering microscopies," ChemBioChem **7**(12), 1895–1897 (2006).
6. K. Wang, C. W. Freudiger, J. H. Lee, B. G. Saar, X. S. Xie, and C. Xu, "Synchronized time-lens source for coherent Raman scattering microscopy," Opt. Express **18**(23), 24019–24024 (2010).
7. R. S. Lim, A. Kratzer, N. P. Barry, S. Miyazaki-Anzai, M. Miyazaki, W. W. Mantulin, M. Levi, E. O. Potma, and B. J. Tromberg, "Multimodal CARS microscopy determination of the impact of diet on macrophage infiltration and lipid accumulation on plaque formation in ApoE-deficient mice," J. Lipid Res. **51**(7), 1729–1737 (2010).

#156640 - $15.00 USD Received 17 Oct 2011; revised 2 Dec 2011; accepted 5 Dec 2011; published 14 Dec 2011

8. Y. Zeng, B. Saar, M. Friedrich, F. Chen, Y.-S. Liu, R. Dixon, M. Himmel, X. Xie, and S.-Y. Ding, "Imaging lignin-downregulated alfalfa using coherent anti-Stokes Raman scattering microscopy," BioEnergy Res. **3**(3), 272–277 (2010).
9. G. Agrawal, *Nonlinear Fiber Optics,* 3rd ed. (Academics Press, 2001).
10. P. Russell, "Photonic crystal fibers," Science **299**(5605), 358–362 (2003).
11. J. K. Ranka, R. S. Windeler, and A. J. Stentz, "Optical properties of high-delta air silica microstructure optical fibers," Opt. Lett. **25**(11), 796–798 (2000).
12. K. M. Hilligsøe, T. Andersen, H. Paulsen, C. Nielsen, K. Mølmer, S. Keiding, R. Kristiansen, K. Hansen, and J. Larsen, "Supercontinuum generation in a photonic crystal fiber with two zero dispersion wavelengths," Opt. Express **12**(6), 1045–1054 (2004).
13. I. Hartl, X. D. Li, C. Chudoba, R. K. Ghanta, T. H. Ko, J. G. Fujimoto, J. K. Ranka, and R. S. Windeler, "Ultrahigh-resolution optical coherence tomography using continuum generation in an air-silica microstructure optical fiber," Opt. Lett. **26**(9), 608–610 (2001).
14. P. Falk, M. H. Frosz, O. Bang, L. Thrane, P. E. Andersen, A. O. Bjarklev, K. P. Hansen, and J. Broeng, "Broadband light generation at approximately 1300 nm through spectrally recoiled solitons and dispersive waves," Opt. Lett. **33**(6), 621–623 (2008).
15. H. N. Paulsen, K. M. Hilligsøe, J. Thøgersen, S. R. Keiding, and J. J. Larsen, "Coherent anti-Stokes Raman scattering microscopy with a photonic crystal fiber based light source," Opt. Lett. **28**(13), 1123–1125 (2003).
16. A. F. Pegoraro, A. Ridsdale, D. J. Moffatt, J. P. Pezacki, B. K. Thomas, L. Fu, L. Dong, M. E. Fermann, and A. Stolow, "All-fiber CARS microscopy of live cells," Opt. Express **17**(23), 20700–20706 (2009).
17. J. X. Cheng, L. D. Book, and X. S. Xie, "Polarization coherent anti-Stokes Raman scattering microscopy," Opt. Lett. **26**(17), 1341–1343 (2001).
18. F. Lu, W. Zheng, and Z. Huang, "Phase-controlled polarization coherent anti-Stokes Raman scattering microscopy for high-sensitivity and high-contrast molecular imaging," J. Opt. Soc. Am. B **25**(11), 1907–1913 (2008).
19. N. K. T. Photonics, femtoWHITE CARS: *http://www.nktphotonics.com/files/files/FWCARS-090612.pdf*.
20. J. C. Knight, T. A. Birks, P. S. J. Russell, and D. M. Atkin, "All-silica single-mode optical fiber with photonic crystal cladding," Opt. Lett. **21**(19), 1547–1549 (1996).
21. A. Ortigosa-Blanch, J. C. Knight, W. J. Wadsworth, J. Arriaga, B. J. Mangan, T. A. Birks, and P. St. J. Russell, "Highly birefringent photonic crystal fibers," Opt. Lett. **25**(18), 1325–1327 (2000).
22. S. Diddams and J. C. Diels, "Dispersion measurements with white-light interferometry," J. Opt. Soc. Am. B **13**(6), 1120 (1996).
23. S. Johnson and J. Joannopoulos, "Block-iterative frequency-domain methods for Maxwell's equations in a planewave basis," Opt. Express **8**(3), 173–190 (2001).
24. M. H. Frosz, P. Falk, and O. Bang, "The role of the second zero-dispersion wavelength in generation of supercontinua and bright-bright soliton-pairs across the zero-dispersion wavelength," Opt. Express **13**(16), 6181–6192 (2005).
25. K. L. Corwin, N. R. Newbury, J. M. Dudley, S. Coen, S. A. Diddams, K. Weber, and R. S. Windeler, "Fundamental noise limitations to supercontinuum generation in microstructure fiber," Phys. Rev. Lett. **90**(11), 113904 (2003).
26. K. L. Corwin, N. R. Newbury, J. M. Dudley, S. Coen, S. A. Diddams, B. R. Washburn, K. Weber, and R. S. Windeler, "Fundamental amplitude noise limitations to supercontinuum spectra generated in a microstructure fiber," Appl. Phys. B **77**(2-3), 269–277 (2003).
27. G. Keiser, *Optical Fiber Communications,* 2nd ed. (McGraw-Hill Science, 1991).
28. T. P. White, R. C. McPhedran, C. M. de Sterke, L. C. Botten, and M. J. Steel, "Confinement losses in microstructured optical fibers," Opt. Lett. **26**(21), 1660–1662 (2001).
29. A. F. Pegoraro, A. Ridsdale, D. J. Moffatt, Y. Jia, J. P. Pezacki, and A. Stolow, "Optimally chirped multimodal CARS microscopy based on a single Ti:sapphire oscillator," Opt. Express **17**(4), 2984–2996 (2009).

1. Introduction

Coherent Anti-Stokes Raman Scattering [1] (CARS) microscopy is a nonlinear imaging technique sensitive to molecular vibrations, where a pump beam and a Stokes beam interact with a sample through the third order susceptibility. When the difference between the pump frequency and the Stokes frequency matches the Raman resonance frequency of the sample, a CARS signal is generated. CARS microscopy is an attractive tool for lipid imaging in tissue where the C-H stretch vibration resonance of 2840 cm^{-1} is excited. In particular, CARS microscopy has been demonstrated successfully in detecting lipid related diseases, such as multiple scleroses [2], atherosclerosis [3] and hepatitis C [4, 5].

Because of the need of two beams, conventional CARS setups have been based on complex systems with two synchronized lasers [6] or optical parametric amplifiers [7,8]. Instead, to provide a simple setup, the wavelengths needed for CARS microscopy may be

#156640 - $15.00 USD Received 17 Oct 2011; revised 2 Dec 2011; accepted 5 Dec 2011; published 14 Dec 2011

generated with a supercontinuum light source. Supercontinuum is typically generated by interplay between several nonlinear effects, such as self-phase modulation, solition fission processes, stimulated Raman scattering, dispersive waves, four-wave mixing and cross-phase modulation [9]. Usually, silica Photonic Crystal Fibers [10] (PCFs) pumped by short pulses in the ps or fs regime are preferred. The properties of high nonlinearities when pumping by using short pulses in conjunction with tailored dispersion profiles of the PCFs, offer the possibility of controlling the output spectra. Pumping the PCF close to a zero-dispersion-wavelength (ZDW) yields efficient broadening of the spectrum, hence, PCF designs having ZDWs in the wavelength region of a fs Ti:Sapphire laser are attractive [11, 12].

PCFs with a single ZDW have been used for several applications, where a broad spectrum is generated and the relevant wavelengths are filtered out subsequently [13]. However, the power of the desired wavelengths might be low compared to the power used to generate the supercontinuum, and the efficiency of the system is low. To alleviate this issue, PCFs have been designed with two ZDWs in order to concentrate the power at specific wavelength ranges [12, 14]. By controlling the structural design of the PCF, mainly pitch size and relative hole diameter, it is possible to control the position of the ZDWs and thereby tailor the spectral distribution of the power at the output of the PCF. Based on such designs, PCFs that concentrate the power at the desired spectral ranges relevant for CARS microscopy have been developed [12].

Previously, CARS setups using PCF for generation of the Stokes wavelength have been presented [15, 16]. However, wavelength conversion to the relevant IR wavelength was weak. Furthermore, the PCFs did not have a polarization maintaining structure. The control of the polarization is an important feature for CARS microscopy, since it is possible to suppress the non-resonant background from electronic contributions to $\chi^{(3)}$ [17] with appropriate alignment of the polarization state of the beams interacting with the sample. With the polarization CARS method Lu et al. [18] have shown a fivefold higher contrast than with conventional CARS for imaging of unstained human epithelial cells.

In this study, we present five different fiber designs with two ZDWs in order to demonstrate the ability to control the spectrum generated in a PCF, i.e., tailoring the generated spectrum for applications in CARS. Based on this study we describe some general guidelines for choosing a suitable PCF design for various input beam parameters. Equally important, the PCF structures are designed in a twofold symmetric structure in order to ensure polarization maintaining (PM) propagation. As mentioned above, this is crucial for further optimization of CARS. For the sake of completeness we compare the novel designs with a PCF having an all-normal dispersion profile.

An experimental procedure for spectral broadening of fs pulses in the PCFs is presented showing the desired control of the output spectrum and its PM properties. The spectral broadening is investigated with the aim of suggesting an optimum PCF candidate for CARS microscopy. In our setup, the PCFs are pumped using a fs Ti:Sapphire laser at center wavelength 795 nm. When this wavelength is used as either the Stokes or the pump beam, we suggest an optimum PCF candidate to generate the second wavelength needed for lipid imaging at either 648 nm or 1027 nm, respectively. This enables a compact system where the generated supercontinuum can be used either as Stokes and pump beam, and the Ti:Sapphire laser can be used as the other wavelength. The CARS signal depends on the pump beam intensity I_P and the Stokes beam intensity I_S as $I_{CARS} \propto I_p^2 I_S$. Therefore, the longer Stokes wavelength is usually generated with the PCF while the more powerful beam obtained directly from the fs-laser is used as the pump. An alternative choice is to use the generated short wavelength as the pump and the laser for the Stokes beam. The use of the shorter wavelengths improves the diffraction limit significantly, hence, the resolution increases [15].

Experiments where the power coupled into the fiber and the fiber length have been varied are presented, and the nonlinear effects in the PCF are analyzed with respect to these

#156640 - $15.00 USD Received 17 Oct 2011; revised 2 Dec 2011; accepted 5 Dec 2011; published 14 Dec 2011

parameters. Furthermore, the observed spectral broadening is compared to numerical solutions of the generalized nonlinear Schrödinger equation (GNLSE) using the split-step method [9]. Finally,the spectral broadening of the optimum PCF is compared to an existing commercially available CARS PCF [19].

2. Photonic crystal fiber designs

We consider six different PCF designs manufactured at NKT Photonics A/S. The fibers are made in pure silica and produced by the stack and draw technique [20]. The nonlinear coefficients of all fibers are relatively large, i.e., in the range of 0.13-0.15 $W^{-1}m^{-1}$. Finally, a twofold symmetric cladding structure provides birefringence, thus, the desired polarization maintaining behavior [21]. A microscope image of one of the structures is shown in Fig. 1. The two larger holes near the core induce birefringence that was measured to be 1.5 10^{-3} using white light interferometry [22].

The main design parameters for each PCF are shown in Table 1. The PCFs are labeled such that the pitch, Λ, decreases with the PCF number. The relative hole diameter, d/Λ, decreases slightly as well. The MIT Photonics Bands package [23] was used to calculate the dispersion profiles for each PCF with the parameters given in Table 1. The six calculated dispersion profiles are shown in Fig. 2. It is seen that the PCFs 1 to 5 have two ZDWs and the separation between the ZDWs decreases. PCF 6 has an all normal dispersion profile.

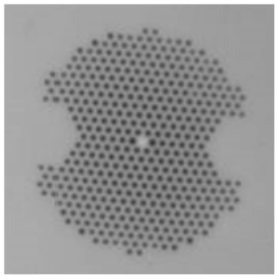

Fig. 1. Microscope image of PCF cross section.

Table 1. Structural parameters of the six PCFs.

PCF no	Pitch *Λ*, µm	Relative hole diameter, *d/Λ*	Position of first ZDW, nm	Position of second ZDW, nm
PCF 1	1.13	0.57	773	1138
PCF 2	1.07	0.56	782	1030
PCF 3	1.05	0.56	783	1001
PCF 4	1.00	0.56	800	916
PCF 5	0.96	0.56	803	867
PCF 6	0.90	0.55	-	-

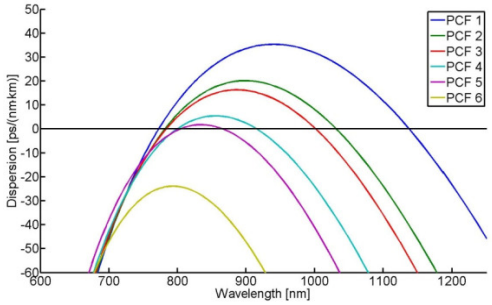

Fig. 2. Dispersion profiles of the PCFs calculated from the parameters given in Table 1.

#156640 - $15.00 USD Received 17 Oct 2011; revised 2 Dec 2011; accepted 5 Dec 2011; published 14 Dec 2011

3. Setup

The setup used for supercontinuum generation in the PCFs is shown in Fig. 3. A commercial fs laser system (FEMTOLASERS Produktions GmbH) centered at 795 nm was used to produce pulses of 11 fs at the output of the laser. Due to temporal dispersion of the optical components, mainly from the microscope objective, the pulse width in focus of the microscope objective is expected to be longer. By using a tunable dispersion compensator (MOSAIC Pro V, setting II = −1650 fs^2) the temporal dispersion was compensated. The pulse width was measured with an autocorrelator (FEMTOLASERS, FemtoMeter) in the focus of the objective to be 89 fs. The input average power is controlled by inserting neutral density filters, and the input polarization is controlled by using a λ/2-plate. The PCFs implemented in the setup were SM fibers with high NAs larger than 0.4. For optimal coupling into the PCFs, a 40X / 0.65-NA microscope objective is used. The output light is collimated with an NIR coated lens having an NA of 0.68 and a focal length of 3.1 mm. The collimated light is collected with a Fiber Optical Integrating Sphere (FOIS, Ocean Optics) and fed to an Optical Spectrum Analyzer (OSA, Ando AQ-6315E) with a 600-µm-core MM fiber.

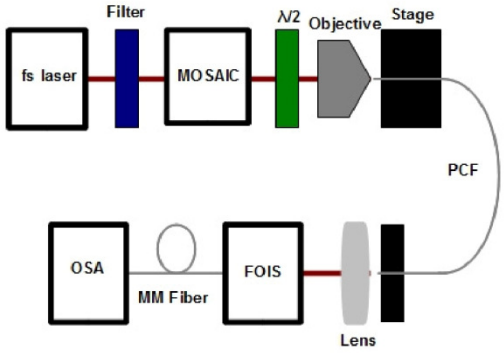

Fig. 3. Ti:Sapphire fs laser (795 nm center wavelength); FemtoSource Compact from FEMTOLASERS; Neutral density filter; MOSAIC dispersion compensator; λ/2-plate; 40X / NA 0.65 microscope objective; 3d translation stage; Photonic Crystal Fiber (PCF); NA 0.68, f −3.1 collimating lense; Fiber Optical Integrating Sphere (FOIS); 600 µm MultiMode (MM) coupling fiber; Optical Spectrum Analyser (OSA).

4. Results

We experimentally investigated the six PCF designs by inserting each of them in the setup with 35 mW of average power coupled to the core. The measured spectra are shown in Fig. 4. The ZDWs and the central wavelength of the Ti:Sapphire laser, λ_0 = 795nm, are shown together with the spectra as the dashed and the dotted lines, respectively. The spectra from PCFs 1 to 4 show similar spectral shapes, in which the light is distributed in three main regions: a sharp blue-shifted signal, a broad central region and a weak red-shifted signal. In agreement with [24], the observed blue-shifted and red-shifted signals on each side on the anomalous dispersion region (ADR) are dispersive waves. The central region of the spectrum is comprised by soliton formation in the ADR. It is seen how the coupling to dispersive waves in the blue-shifted region increases when the first ZDW is positioned closer to the pump wavelength. Thereby an increasing signal in the blue-shifted region is observed. When the second ZDW moves to shorter wavelengths the broad central signal gets narrower, i.e., the second ZDW prevents further red-shifting of the central spectrum. In the case of PCF 5, the ADR is sufficiently narrow and only two peaks are observed in the generated spectrum. The generated solitons “recoil” out of the ADR and stabilize in the normal dispersion regime (NDR). The red-shifted peak moves further to IR due to stimulated Raman scattering. For the sake of completeness, PCF 6 generates a spectrum mainly distributed in two weakly separated

#156640 - $15.00 USD Received 17 Oct 2011; revised 2 Dec 2011; accepted 5 Dec 2011; published 14 Dec 2011

peaks. Because of the all-normal dispersion profile, the broadening is purely caused by self-phase modulation.

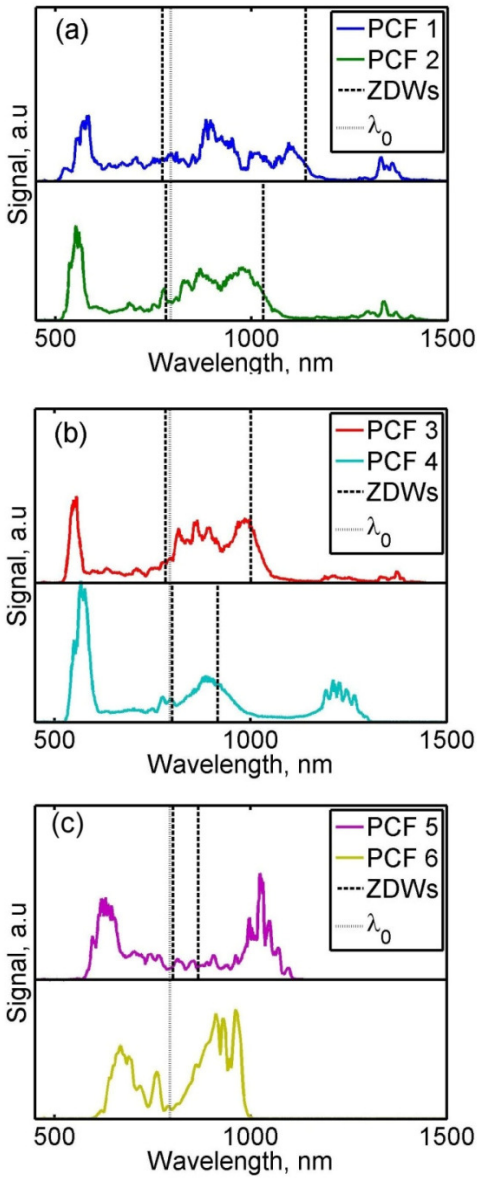

Fig. 4. Spectra measured from (a) PCF 1 and PCF 2, (b) PCF 3 and PCF 4, (c) PCF 5 and PCF 6. All spectra are measured with a PCF length from 35 cm to 40 cm and with a coupled average power of approximately 35 mW.

Selection of optimum PCF for CARS

Based on the observations above, it is possible to set some general guidelines for selecting an optimal PCF for CARS. First, the separation of the two ZDWs must be sufficiently narrow to generate a dual-peak spectrum at the desired wavelengths. Second, the pump wavelength should be centered close to the first ZDW in order to achieve an efficient broadening of the spectrum [14]. In addition, it is required that the anomalous dispersion is sufficiently low between the two ZDWs in order to efficiently initiate self-phase modulation. Too high

#156640 - $15.00 USD Received 17 Oct 2011; revised 2 Dec 2011; accepted 5 Dec 2011; published 14 Dec 2011

dispersion broadens the pulses in time and, thus, inhibits the nonlinear process needed for spectral broadening.

When using the central wavelength of the Ti:Sapphire laser of 795 nm as one of the wavelengths in the CARS process, the second wavelength should be chosen at 1027 nm or 648 nm for imaging lipids. Around these wavelengths two relevant CARS regions are defined to be within 648 nm ± 15 nm and 1027 nm ± 20 nm, where a Raman linewidth of 100 cm^{-1} and the possibility of some tunability have been taken into account. The conversion efficiencies to the CARS regions are shown in Table 2. PCF 5 renders itself a suitable candidate as a CARS source based on its spectral properties: in the NDR a spectrum with the power distributed in the two ranges around the relevant wavelengths is generated, hence showing the most efficient conversion of 12.1% and 16.9% to relevant CARS wavelengths in the blue-shifted and the red-shifted region, respectively. In agreement with [24] the dominating effects are soliton fission processes, generation of dispersive waves and stimulated Raman scattering. In the case of PCF 6 where no solitons are generated, the spectral broadening is insufficient. In the case of PCF 1 to 4, the ADR is too wide and the solitons stay in the ADR. This gives simultaneously a blue-shifted dispersive wave at wavelengths shorter than relevant for CARS microscopy.

In the following we will focus on characterizing PCF 5 as it seems the optimum candidate for an improved CARS fiber.

Table 2. Conversion efficiencies to relevant wavelengths

PCF no	Blue-shifted conversion efficiency, %	Red-shifted conversion efficiency, %
PCF 1	2.7	5.6
PCF 2	1.6	6.6
PCF 3	2.0	6.7
PCF 4	1.8	1.4
PCF 5	12.1	16.9
PCF 6	8.7	0.01

Fixed pulsewidth, decreased peak power

In Fig. 5 it is shown how the spectrum from PCF 5 changes when varying the coupled average power. The pulse width measured in focus of the objective is 89 fs. In order to consider the shape of the spectra, the measurements are normalized to the total area, i.e., the total coupled power. The average power was varied by changing the neutral density filter seen on Fig. 3. The power coupled to the PCF is measured with a powermeter at the PCF output. In general, it is seen how the spectrum narrows with less average power coupled to the PCF. However, the two peaks at 648 nm and 1027 nm are still visible until the average power is attenuated to 3.6 mW. Moreover, less light is converted when the average power is lower than 17 mW. When the average power has been decreased to 0.60 mW, the pulse is only broadened slightly from self-phase modulation.

#156640 - $15.00 USD Received 17 Oct 2011; revised 2 Dec 2011; accepted 5 Dec 2011; published 14 Dec 2011

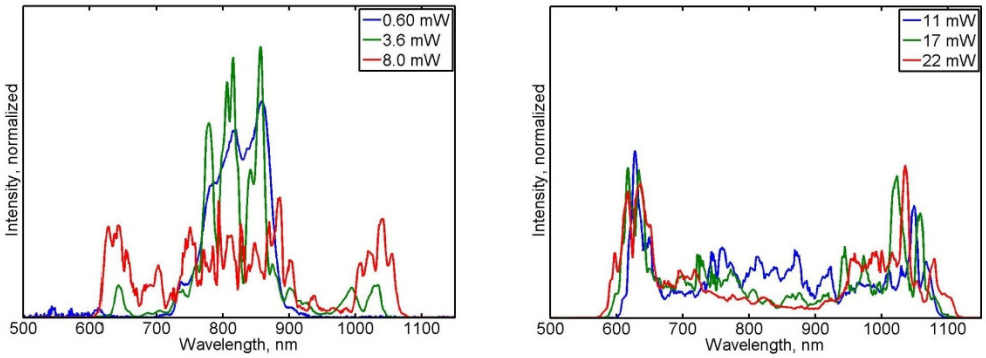

Fig. 5. Spectra measured with average power varied from 0.60 mW to 8.0 mW (left) and 11 mW to 22 mW (right).

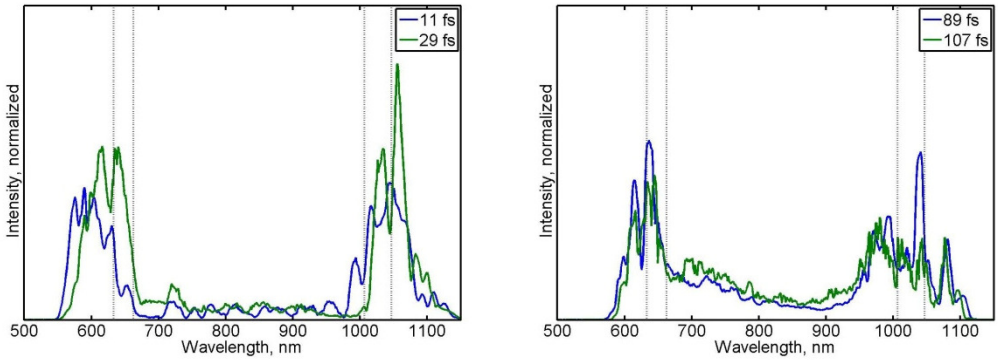

Fig. 6. Spectra measured with the input pulse duration of 11 fs and 29.0 fs (left), and 89 fs and 107 fs (right). The dotted lines indicates the relevant CARS wavelengths around 648 nm ± 15 nm and 1027 nm ± 20 nm.

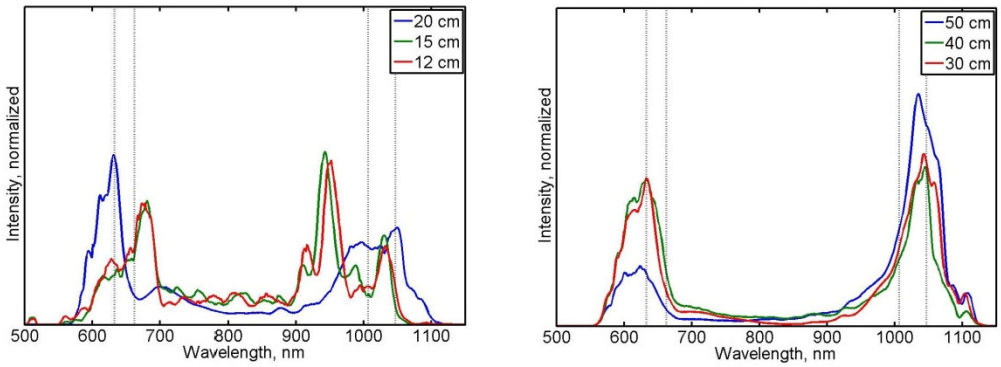

Fig. 7. Spectra measured from PCF 5 when the length is varied from 12 cm to 20 cm (left) and 30 cm to 50 cm (right). The dotted lines indicates the relevant CARS wavelengths around 648 nm ± 15 nm and 1027 nm ± 20 nm.

Varying the pulse width

Figure 6 shows the spectral broadening when changing the pulse width and thereby the peak power for a fixed average power of 22 mW. The relevant wavelength regions for CARS microscopy around 648 nm and 1027 nm are also shown. The chirp of the input pulse was controlled with the MOSAIC dispersion compensator and some additional glass plates in the setup. The pulse width was measured with an autocorrelator in focus of the microscope

#156640 - $15.00 USD Received 17 Oct 2011; revised 2 Dec 2011; accepted 5 Dec 2011; published 14 Dec 2011

objective. In the standard setup with the MOSAIC setting II and no additional glass the pulse width was measured to be 89 fs. When the pulse width is shortened compared to this, the spectrum broadens further in the blue-shifted wavelength region due to an increase in the peak power. Some broadening in the red-shifted region is observed as well, but the power conversion efficiency to the relevant CARS wavelengths is not changed significantly. One spectrum was measured also with a longer pulse width where the MOSAIC setting III (−2310 fs^2) was used. For the pulse width of 107 fs, the wavelength conversion was found to decline when compared to the standard setting. In general, shortening the pulse width improves conversion to the blue-shifted and the red-shifted peaks. Unfortunately, in our experiment with PCF 5 the blue-shifted signal moves out of the relevant wavelength region when the shortest pulses are used. As a trade-off, for a simultaneously efficient conversion to both the relevant wavelength regions, the pulse width of 89 fs was chosen.

Chirped pulses have been found to alter the output spectrum and introduce noise when compared to pumping with transform limited pulses [25, 26]. However, based on an earlier study with a double-ZDW fiber similar to ours, we expect the chirp of the input pulses to have only a minor effect on the output spectrum [12]. Furthermore, in the same study the noise in the output spectrum from this type of a PCF was measured to be lower than the one reported for standard PCFs.

Cutback measurements

In Fig. 7 the length of the PCF has been varied. The fiber output spectra were measured using the cutback method, i.e. the setup was fixed except for the fiber length. The spectra are again normalized to the total, coupled power calculated from each spectrum. It is clearly seen how the IR peak shifts to longer wavelengths when the fiber length is increased, which is caused by Stimulated Raman Scattering. Also the shape of the peaks varies when changing the fiber length. Considering the IR peak, the most suitable spectrum for CARS microscopy is from 20 cm to 50 cm, but because of fiber losses, i.e. signal attenuation from mechanisms as absorption, scattering [27] and confinement losses [28], it is convenient to choose the shortest possible fiber length. For this reason a length of 28 cm is chosen for the following experiments.

Polarization maintaining properties

Existing commercially available CARS PCFs are not designed for PM propagation. If the polarization is maintained in the PCF, no polarization filtering is necessary after the PCF for CARS excitation, i.e., no excitation power loss. Furthermore, as discussed in the introduction, polarization of the excitation light is important due to the improved signal-to-noise for the resulting CARS signal due to non-resonant background suppression. Accordingly, an important motivation for the new design, and thus this study, was to investigate the PM properties of the novel design. It was experimentally verified that the input polarization state was maintained by inserting a λ/2-plate and a polarizing beam splitter (PBS) at the PCF output. Transmitted polarization state contained 93% of the light, while 7% was reflected in the PBS. Taking the imperfect optics for broadband light sources (PBS is coated for 650-900 nm) into account, we conclude that the PCF is polarization maintaining.

Numerical calculation of pulses evolving in PCF

In order to investigate the spectral broadening when pulses propagate in a PCF, the split-step Fourier method [6] is used to solve the generalized nonlinear Schrödinger equation

$$\frac{\partial A(z,t)}{\partial z} = \hat{D}A(z,t) + i\gamma\left[1+\frac{i}{\omega_0}\frac{\partial}{\partial t}\right]\left[A(z,t)\int_{-\infty}^{t} R(t')\,|\,A(z,t-t')\,|^2\,dt'\right],$$

#156640 - $15.00 USD Received 17 Oct 2011; revised 2 Dec 2011; accepted 5 Dec 2011; published 14 Dec 2011

where *A(z,t)* is the pulse envelope moving in the retarded time frame *t* with the group velocity of the pump along the z-axis. $\hat{D}$ is the operator from where the dispersion of the PCF acts on the pulse given as $\hat{D} = i\sum_{m\geq 2} \frac{i^m \overline{\beta}_m}{m!} \frac{\partial^m}{\partial t^m}$. The dispersion coefficients of PCF 5 are calculated with the MIT Photonics Bands package of the design with the pitch and the relative hole diameter given in Table 1. $R(t')$ is the Raman response function.

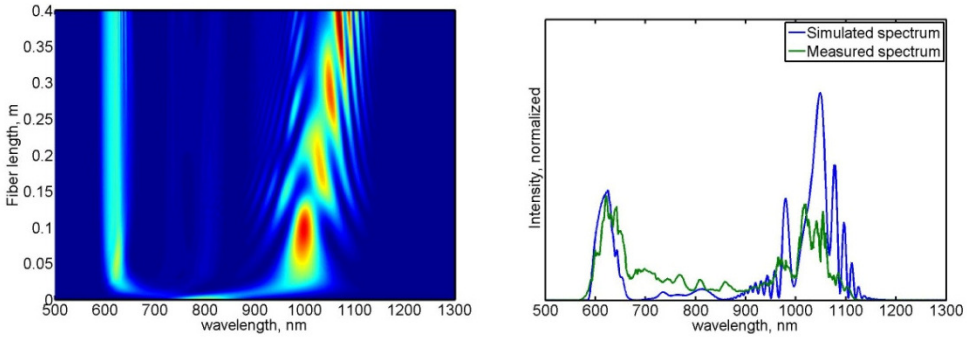

Fig. 8. Numerical calculation of an 11 fs pulse propagating in PCF 5, where red indicates high intensity (left), and the simulated spectrum together with measured spectrum after 28 cm of propagation in PCF 5 (right).

Figure 8 (left) shows the simulated spectral broadening of a Gaussian pulse in PCF 5. The input pulse has a temporal width of 11 fs comparable to the pulses from the Ti:Sapphire laser. The peak power of the input pulse was set to be 4 kW. The pump pulses have a repetition rate of 75 MHz yielding a coupled average power of 29 mW, in agreement with our experimental observation. It is seen how the pulse immediately broadens to a blue-shifted dispersive wave and red-shifted solitons that are further red-shifted by stimulated Raman scattering. Figure 8 (right) shows the spectrum calculated with the split-step method after 28 cm propagation (blue curve) and the measured spectrum at the same distance of propagation (green curve), respectively. The broadening of the two spectra is comparable. The power coupled to the fiber was approximately 35 mW, although some power is expected to be lost to cladding modes. The intensity of the IR region is seen to be higher in the simulated case than for the measured spectrum. This was also observed in [12], and it is mainly expected to be caused by confinement losses [28].

Varying the pump wavelength

The experimental studies were carried out with the pump wavelength centered at 795 nm. However, the generated spectrum is expected to be dependent on the center wavelength of the pump. For this reason it was investigated numerically how the spectrum changes when pumping PCF 5 at different center wavelengths. In Fig. 9 (left) calculated spectra are shown when pumping by center wavelengths at both sides of the first ZDW, i.e. at NDR (λ_0 = 775 nm and λ_0 = 795 nm) and ADR (λ_0 = 815 nm). Other parameters of the pulse and the PCF are the same as in the previous section. It is seen that the spectrum broadens more when the center wavelength of the pump is increased. For all three cases, the red-shifted peak stays in the regime where it is useful as a Stokes wavelength, since the ideal Stokes wavelength is shifted towards longer wavelengths, when the pump wavelength increases. The black lines indicate the ideal Stokes wavelength for the shortest and the longest pump wavelength, respectively. From the three shown curves in Fig. 9 (left), it is seen that 795 nm is preferred as the center wavelength because of the best power conversion to the relevant regimes, but minor deviations within ± 15 nm are not considered critical. This insensitivity to variations of the

#156640 - $15.00 USD Received 17 Oct 2011; revised 2 Dec 2011; accepted 5 Dec 2011; published 14 Dec 2011

center wavelength when pumping close to the first ZDW is explained by the small change in the absolute dispersion value when moving from the NDR to the ADR. Fig. 9 (right) shows spectra calculated with λ_0 = 840 nm and λ_0 = 880 nm. In the case of λ_0 = 840 nm, the center wavelength of the pump is close to the vertex of the dispersion curve. We observe no broadening to relevant CARS wavelengths with this pump wavelength, and we exclude further studies of this case. The center wavelength of λ_0 = 880 nm is in the vicinity of the second ZDW. Again, the broadening to the regimes relevant as Stokes wavelength is limited and the spectrum exhibits also large ripple compared to the red-shifted peak generated when pumping close to the first ZDW. At the same time it should be noted that loss mechanisms are not included in the simulations. In particular confinement loss may prevent the use of the longer wavelengths as the Stokes wavelength.

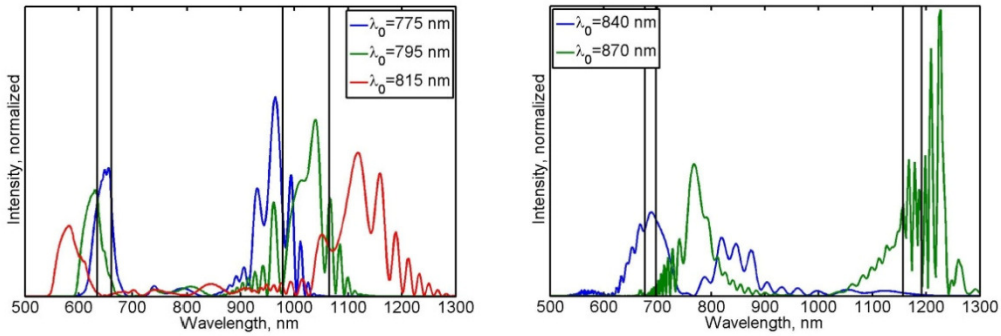

Fig. 9. Calculated spectra with the pump wavelength centered close to the first ZDW (left) and at 840 nm and 870 nm representing pump wavelengths in the middle of the ADR and close to the second ZDW, respectively (right).

Optimum PCF for CARS

The spectrum generated from PCF 5 was compared to a spectrum generated from a commercially available CARS PCF 'femtoWHITE CARS' produced by NKT Photonics A/S. In both cases the coupled average power of the pump light was 35 mW, which was the maximum power available in our experiment. The commercial PCF was designed to a length of 12 cm whereas PCF 5 had a length of 28 cm. Figure 10 shows the spectra from PCF 5 and 'femtoWHITE CARS', respectively. It is seen how the broadening of the two spectra are comparable, but the spectrum from PCF 5 has its power concentrated in two peaks around the relevant CARS wavelengths. The spectrum from 'femtoWHITE CARS' has, especially in the red-shifted wavelength region, a non-localized distribution of power, hence, the power for the actually needed wavelength in the CARS process is low. With the power distribution of the spectrum of PCF 5, the power of the second wavelength in the CARS process generated with the PCF is increased. The highest spectral densities for relevant CARS wavelengths generated with PCF 5 were measured to be 201 µW/nm and 206 µW/nm for blue-shifted and red-shifted wavelengths, respectively. In addition, PCF 5 generates a spectral power density higher than 100 µW/nm for all relevant CARS wavelengths. CARS experiments have successfully been performed with 'femtoWHITE CARS' where 12 mW of power was achieved when using the red-shifted part of the spectrum as Stokes beam, while the blue-shifted peak was filtered away [29]. With the improved power distribution, an enhanced CARS signal can be achieved when using PCF 5 i.e. a faster imaging process than achieved with other PCF based CARS systems (4 µs/pixel) [16]. Note that the commercially available fiber is not polarization maintaining.

#156640 - $15.00 USD Received 17 Oct 2011; revised 2 Dec 2011; accepted 5 Dec 2011; published 14 Dec 2011

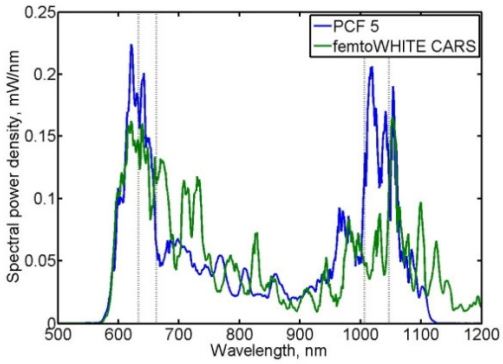

Fig. 10. Spectra measured from PCF 5 (blue curve) and 'femtoWHITE CARS' (green curve). Both spectra are measured with 35 mW of coupled average power, and are normalized to this.

5. Conclusion

In conclusion, we have investigated PCF designs with two ZDWs in order to suggest a novel PCF design for generating the second wavelength needed for CARS microscopy. From this investigation, we select the optimum PCF design having the pitch size of $\Lambda = 0.96$ μm and the relative hole diameter of $d/\Lambda = 0.56$, respectively. Spectral broadening covering relevant CARS wavelengths at 648 nm and 1027 nm was demonstrated experimentally with sufficient power conversion efficiency. Simultaneously, the PCF had a twofold symmetric structure ensuring polarization maintaining propagation, which was experimentally verified. The PCF design was characterized by varying the input parameters, i.e., average power, pulse width and PCF length. By using pulses from a Ti:Sapphire laser of 89 fs, centered at 795 nm, and a coupled average power of 35 mW to the PCF of length 28 cm, a spectrum with power concentrated at the relevant wavelengths was generated. Furthermore, the measured spectrum was in good agreement with numerical calculations, and from this, it was found that the nonlinear effects responsible for the spectral broadening are due to soliton fission processes, dispersive waves and stimulated Raman scattering.

The spectrum generated from the novel, optimum PCF was compared to a spectrum generated from a commercially available CARS PCF. We demonstrated enhanced power distribution localized at the relevant IR wavelengths as well as maintaining of the polarization state for the new CARS PCF. It is expected that the increased power gives an enhanced CARS signal and thereby a faster imaging than previously achieved with the commercially available CARS PCF. Equally important is that the polarization maintaining propagation provides an improvement in the signal-to-noise ratio in CARS applications.

Acknowledgments

The authors acknowledge Dr. Michael Frosz for fruitful discussions and assistance in numerical calculations of the dispersion curves.

#156640 - $15.00 USD Received 17 Oct 2011; revised 2 Dec 2011; accepted 5 Dec 2011; published 14 Dec 2011